A New Radiosonde System for Profiling the Lower Troposphere

BRIAN R. CORNER AND ROBERT D. PALMER

Department of Electrical Engineering and Center for Electro-Optics, University of Nebraska at Lincoln, Lincoln, Nebraska

MIGUEL F. LARSEN

Department of Physics and Astronomy, Clemson University, Clemson, South Carolina

(Manuscript received 11 January 1998, in final form 5 October 1998)

ABSTRACT

A new, inexpensive radiosonde transmitter and receiver system has been developed for measuring wind field inhomogeneities in the planetary boundary layer using multiple simultaneously launched balloons. The radiosondes use a narrowband-frequency-modulated carrier signal to transmit atmospheric pressure and temperature information to a surface receiver. The pressure and temperature data transmitted by the radiosondes allow their height above the surface to be ascertained. In addition, the radiosondes can be tracked with a photographic camera system to provide the azimuth and elevation angles of the radiosondes during their ascent, so that their three-dimensional horizontal position can be determined. By tracking the spatial separation of the radiosondes over time, horizontal gradients can be derived. The system hardware and results from preliminary tests are described.

1. Introduction

Radiosondes and rawinsondes have been used extensively for profiling the troposphere and lower stratosphere for both experimental and operational purposes. A global network performs launches twice daily to obtain upper-air information for synoptic-scale forecasting. Experimental studies often involve specialized balloon payloads such as the ones developed by Dalaudier et al. (1994) to obtain detailed measurements with altitude resolutions as small as 20 cm. A single radiosonde ascent clearly can provide important information, but multiple radiosondes launched simultaneously can provide additional information about the horizontal gradients in the thermodynamic parameters and in the winds. Jasperson (1982) performed such measurements to determine the horizontal and temporal correlation scales. Such measurements can, in principle, be performed with equipment that is available commercially, but the cost of purchasing the expendable radiosondes and, in particular, the ground-receiving equipment is high. This is particularly evident when at least three commercial receiving units are required for the system. In this note we describe a new, inexpensive radiosonde system that has been developed for tropospheric profiling. The system allows three or more radiosondes to be launched simultaneously to measure small-scale horizontal gradients in atmospheric parameters. The initial goal of the new system is the in situ verification of Doppler radar vertical velocity measurements using derived divergence estimates from the balloon network. The initial tests of the system were described by Corner (1997).

Radiosondes have the important capability of acquiring in situ measurements of atmospheric parameters. With this new radiosonde system, in conjunction with a photographic tracking system, in situ measurements of not only pressure and temperature are available but also horizontal velocity divergence, vertical winds, relative vorticity, and horizontal winds and other inhomogeneities. From the pressure and temperature information obtained by the radiosondes, their height above the surface can be calculated. Optically tracking the balloons over time using a photographic camera system provides the azimuth and elevation angles that, along with the height information, allows the three-dimensional positions of the balloons to be determined. The radiosondes can be tracked by the cameras throughout the boundary layer before the balloon images become too small to be discerned in the photographs. The hardware developed for this system was designed to operate in the 2-m amateur radio band. Because of this frequency selection, the electrical components and receiver equipment used in the system are readily available and relatively inexpensive. With the radiosonde system, in

Corresponding author address: Brian R. Corner, Department of Electrical Engineering, 209 North Walter Scott Engineering Center, P.O. Box 880511, Lincoln, NE 68588-0511.

situ atmospheric information can be obtained for a fraction of the cost that would be required using commercially produced radiosondes and tracking equipment.

In this note, the design of the radiosonde system hardware will be described, including calibration procedures. Preliminary data will also be presented in comparison with National Weather Service (NWS) radiosondes to validate the system operation. Finally, possible applications for the instrumentation will be discussed.

2. Hardware description

a. Design considerations

The carrier frequencies chosen for the radiosondes are in the range 144–148 MHz, which is within the 2-m amateur radio band. Federal Communication Commission (FCC) regulations require a technician class or higher amateur radio license for transmission in the 2-m band (United States Federal Communications Commission 1995). Part 97 of the FCC regulations govern amateur radio operation and place limitations on the design of the radiosondes. The radiosondes are a form of the manually controlled beacon station in that they transmit for the purposes of experimental activities. FCC regulations for a manually controlled beacon station state that the transmitted power of the beacon must be less than 100 W and that beacons are allowed to transmit one-way communications of telemetry. The transmissions of the radiosondes are permitted within 50 km of the surface and, as they are telemetry, are not considered to be codes or ciphers, which are disallowed by the FCC. The beacon station must also identify itself by transmitting the call sign of the control operator of the station at least once every 10 min.

The Federal Aviation Administration (FAA) also has regulations pertaining to the use of moored balloons and unmanned free balloons (United States Federal Aviation Administration 1994). Part 101 of the FAA regulations state in summary that any unmanned balloon is subject to the regulations if it carries a payload weighing more than 4 lb or if it requires an impact force of more than 50 lb to separate the payload from the balloon. The radiosondes described here do not exceed either of these requirements and adhere to all relevant FAA regulations.

b. Radiosonde system

The radiosonde system has been designed to measure temperature and pressure and to transmit the call sign of the control operator at least once every 10 min, as required. A time-division multiplexing (TDM) scheme was implemented in order to accomplish the various tasks. The block diagram of the transmitter system is shown in Fig. 1. A complete circuit diagram of the TDM portion of the radiosonde transmitter is shown in Fig. 2. The main component of the radiosonde transmitter is

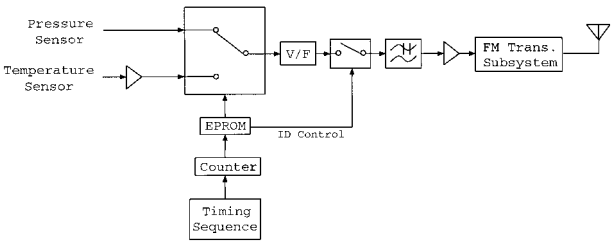

FIG. 1. Block diagram of the TDM radiosonde transmitter circuitry. The EPROM controls a digital switch that implements the multiplexing. The voltages of the multiplexed data are converted to an audio frequency, low-pass filtered, and amplified before modulating the transmitted carrier. During the identification process, the EPROM controls a second switch operating on the pressure data to produce only a Morse code sequence. This second switch is closed during normal operation.

the MC2833P integrated circuit (IC), which is a crystal-controlled, single-chip, narrowband FM transmitter system with a maximum power output of 5 dBm at 144 MHz. The FM transmitter circuit diagram is given in Fig. 3. The IC has built-in RF amplification and modulation capabilities that satisfy all of the requirements for the transmission without the need for additional subsystems. The MC2833P multiplies the frequency of the external crystal by a factor of 12 in order to generate the RF signal. Using 12.0-, 12.096-, and 12.288-MHz crystals produces transmitted frequencies of 144.0, 145.152, and 147.456 MHz, respectively. A tunable inductor in series with the crystal allows the final transmitted frequency to be varied by a few tens of kilohertz. Power is supplied to the transmitter by two 9-V batteries.

The transmission antenna is a vertically polarized, center-fed, $\lambda/2$ dipole mounted on the side of the radiosonde transmitter container, with λ being the transmitted wavelength. A section of RG174/U coaxial cable was used, with the outer conductor cut away from the inner conductor on the upper $\lambda/4$ section. The outer conductor is then pulled back over the feed portion of the coax to make the antenna. Each section is $\lambda/4$ in length and becomes half of the overall length of the antenna.

The radiosondes measure temperature with the LM135AH IC temperature sensor. This sensor produces an output voltage proportional to the absolute temperature in the linear ratio of 10 mV K^{-1}. The typical calibrated accuracy of the sensor, as stated by the manufacturer, is 0.3°C, with a time constant of approximately 5 s in moving air over the temperature range of $+100°$ to -55°C. Laboratory testing showed this specified accuracy to be realistic. The sensor is mounted on a mast extending about 0.2 m from the radiosonde payload container.

Pressure sensing is accomplished with the Motorola MPX4115AP absolute pressure sensor, which provides a linear output voltage proportional to atmospheric pressure over a range of 150–1150 hPa. The sensor is an

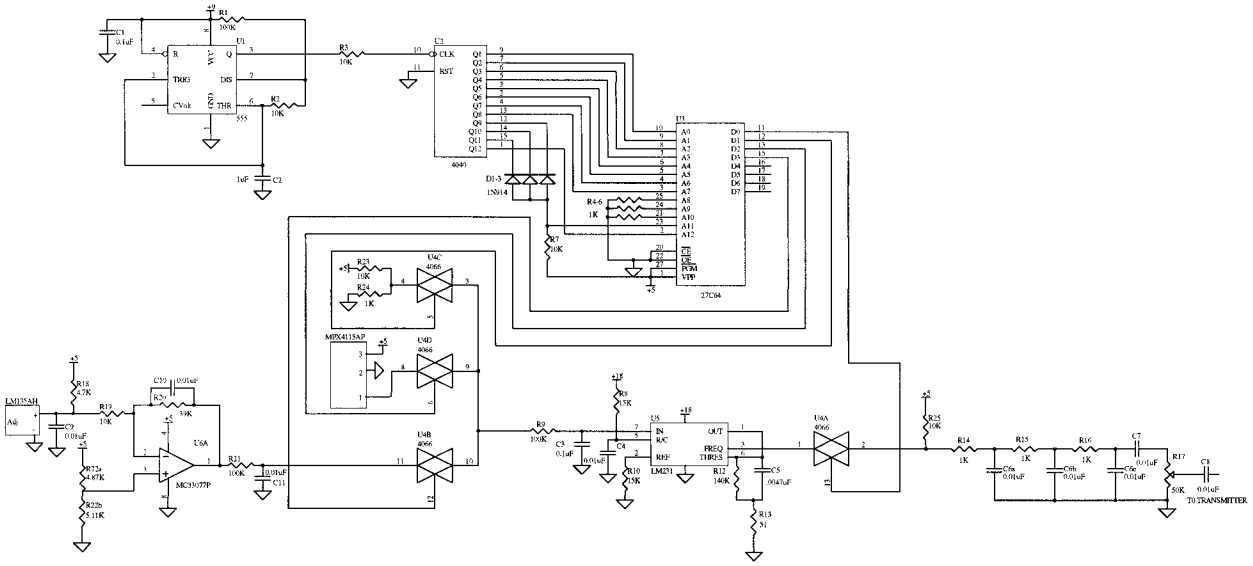

FIG. 2. Circuit diagram of the TDM portion of the radiosonde transmitter. The 27C64 EPROM is the large IC toward the right of the diagram. On the left side of the diagram is the binary counter, frequency-to-voltage converter, and digital switch. The output of this section enters the FM transmitter circuitry given in Fig. 3.

integrated circuit design and contains built-in temperature compensation. The compensation provides a constant temperature error factor over the expected temperature range inside the radiosonde package. Temperature effects on the pressure sensor can then be accounted for in the calibration process. The uncalibrated maximum error of the sensor given by the manufacturer is ± 15 hPa, with a typical response time of 1.0 ms. To obtain a more realistic account of the error after calibration, pressure data were collected from several radiosondes at surface pressure over an approximate 15-min period. The standard deviation of the pressure data from all of the radiosondes was less than 1.0 hPa. This error is comparable to that of NWS radiosondes.

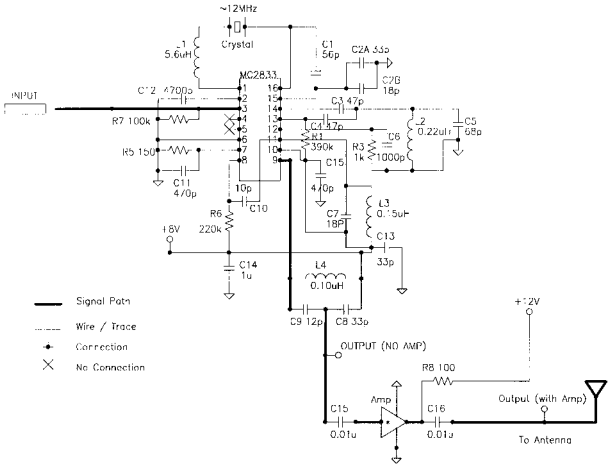

FIG. 3. Circuit diagram of the FM portion of the radiosonde transmitter. Frequency modulation and transmission of the data are performed by this circuit.

The basis for the multiplexing in the TDM circuit design of Fig. 2 is a continuous series of timing pulses produced by a 555 IC timer. The timer runs at approximately 12 Hz and is used as the input for a 4040 binary ripple counter. The ripple counter has 12 outputs and thus provides 2^{12} possible states. The first eight output lines of the 4040 are fed directly into an EPROM. The final four states are used to determine when the call sign identification takes place. Because of the limited number of input lines to the EPROM, three of the 4040 output states are input to an AND gate composed of switching diodes to produce a single input line to the EPROM. When all four of the final states go high, the transmitter will send the identification sequence. The EPROM has 13 total input lines, with 10 of those being supplied by the 12 ripple counter outputs. The remaining three input lines are configured as test inputs. Setting the appropriate test line high disables the multiplexing and produces an output of either temperature or pressure data. This feature is used for calibrating the system.

The EPROM has eight output lines, but only four are used. The four EPROM outputs are the control lines for a 4066 quad bilateral switch. Each switch will remain off with a low input, and turn on when the output of the EPROM on that control line goes high. The pressure and temperature signals enter these switches and are switched on and off in succession by the EPROM to produce the multiplexing. Only one of the pressure and temperature switches is on at one time for eight clock cycles each, respectively. The temperature signal is inverted and amplified using a MC33077P operational amplifier before entering the switch, in order to increase the dynamic range of the temperature sensor.

When the pressure or temperature switch is on, the

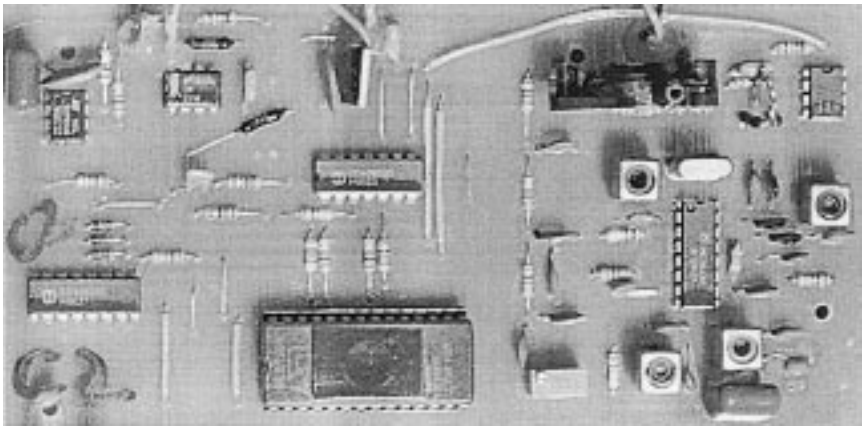

FIG. 4. Photograph of the radiosonde transmitter. The EPROM is the large integrated circuit at the bottom center of the photo. On the left side of the image is the binary counter and frequency-to-voltage converter. To the right of center at the top of the image is the pressure sensor. Just below the pressure sensor is the FM transmitter circuitry. Battery-connection wires and the temperature sensor extend out from the top of the image.

signal enters a LM231 voltage-to-frequency converter that produces a pulse train with a frequency directly proportional to the input voltage. The output of the LM231 then enters the final section of the quad switch. The EPROM again controls the on/off state of this switch, which is on in the normal state of data transmission. However, when the binary counter reaches a state with the last four inputs high and all others low, an identification sequence begins. During the identification, the temperature switch is turned off and only the pressure switch is on. The EPROM then switches the output of the LM231 in a sequence that gives a Morse code identification of the control operator. Because of the clock speed of approximately 12 Hz, each identification in Morse code takes about 6.5 s and corresponds to a Morse code rate of about 15 words per minute. Once the identification ends, the modulation pauses for eight clock pulses before resuming the normal data modulation sequence. Following the LM231, a three-pole cascaded RC low-pass filter stage with a cutoff at 15.9 kHz is needed to remove any high-frequency interference. Finally, the signal enters a deviation adjustment amplifier before being used to modulate the transmitter carrier by the MC2833P. A photograph of the complete radiosonde transmitter is shown in Fig. 4. The entire package, including the printed circuit board, is constructed in house for a cost of less than $150.

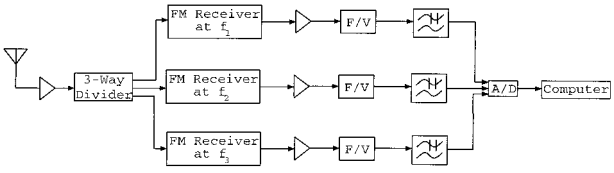

FIG. 5. Block diagram of the radiosonde receiver circuitry. After the transmitted signals are received by a Yagi antenna, the signals are split by a three-way power divider and sent to the three FM receivers. The demodulated audio-signals are then converted back to a voltage and are low-pass filtered before being sampled by an analog-to-digital board and stored in a personal computer.

c. Receiver design

A receiver unit employing commercial handheld receivers and minimal additional circuitry was designed in order to receive simultaneously all of the radiosonde transmissions. The block diagram of the receiver is shown in Fig. 5, while the compact design of the receiver system can be seen in the photograph shown in Fig. 6. The transmitted signals are first received by a three-element Yagi antenna. The antenna is tuned to approximately 146 MHz, which is in the center of the desired band. The receiving antenna is vertically polarized to match the polarization of the radiosonde transmitting antennas. The transmitted signals are passed through a 15-dB low-noise preamplifier, followed by an RF three-way power divider that provides equal-level signal inputs for three handheld receivers. The units are Yaesu FT-50R transceivers and serve to demodulate the received signals. The transceivers were found to be sensitive to input signals as low as -100 dBm which is adequate for the weak received signals from the radiosondes. The transceivers are tunable, of course, which allows them to be tuned to a frequency approximately equal to the frequency of the three transmitters used for simultaneous launches.

The audio signal is amplified using a MC33077P operational amplifier after the received signals are demodulated by the transceivers. The audio frequency of the signal is then converted to a voltage by an LM2917 frequency-to-voltage converter. Finally, the data are low-pass filtered, sampled by an analog-to-digital converter at 100 Hz, and stored on a personal computer. The entire receiver system was developed for less than

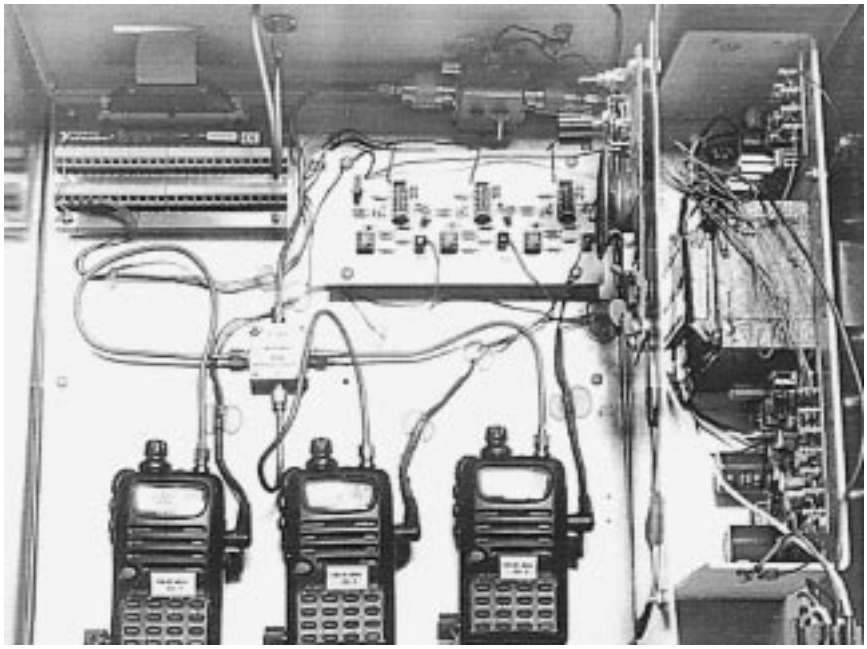

FIG. 6. Photograph of the radiosonde receiver. After being received by a Yagi antenna, the signals enter the receiver box via a semirigid coaxial cable that runs through a preamplifier controller at top and the power divider at center and into the three transceivers. The signal leaving the transceivers is amplified, converted to a voltage, and filtered by the circuitry at top center. The signal then enters the data block at top left that connects directly to the personal computer A/D board. Power is supplied to the receiver system by the power supply on the right side.

$5,000 and can receive all three radiosonde signals in a single unit. The developed receiver is considerably less expensive than any commercial receiver–tracking system, especially considering the fact that at least three of these receiving systems would be required. A conservative estimate of the cost of a commercial system capable of receiving three radiosonde signals would be approximately $75,000.

d. Laboratory calibration

Since each radiosonde transmitter has slightly different outputs because of component tolerances, a calibration procedure is required for each radiosonde–receiver pair. The outputs of the sensors and the other system components vary in a near linear fashion with pressure and temperature changes. The radiosondes can be calibrated by varying the pressure and temperature and recording the voltage outputs of the receivers. Specifically, the calibration procedure is as follows. A hose is connected from the pressure sensor to a pump and high-accuracy digital pressure gauge. The pump is then used to lower the pressure at the sensor, and the voltage at the input to the computer is recorded for numerous pressure values. A least squares polynomial fit to the data then provides the required relationship between the pressure values and the output voltage. A plot showing the typical error of the calibration is given in Fig. 7a. The calibration error ϵ is given as

$$\epsilon = P_c - P, \tag{1}$$

where P_c is the calibrated value and P is the actual measured value. A high-order polynomial is used to fit the calibration data of pressure versus voltage, and results in an oscillation in the calibration error curve. The pressure-calibrated errors are generally less than 0.20 hPa.

A similar procedure is used to calibrate the temperature sensor, although varying the temperature in controlled conditions is more difficult. Obviously, room temperature, ice-bath temperature, and outdoor temperatures can be recorded, but just a few points do not always provide an accurate calibration. In order to improve the calibration, a potentiometer is placed in parallel with the temperature sensor, and its resistance is adjusted to change the sensor output voltage in order to simulate actual temperature changes. Any slight nonlinearities throughout the system are also accounted for in this way. These values can then be used for the fitting procedure and for subsequent calibration. Figure 7b shows a typical plot of the temperature calibration error. Because of slight measurement errors in determining the voltages with the potentiometer, the plot is not as smooth and uniform as is the plot for pressure. However, the calibrated errors are generally less than 0.10°C. Proper calibration of the system is vital to acquire accurate results.

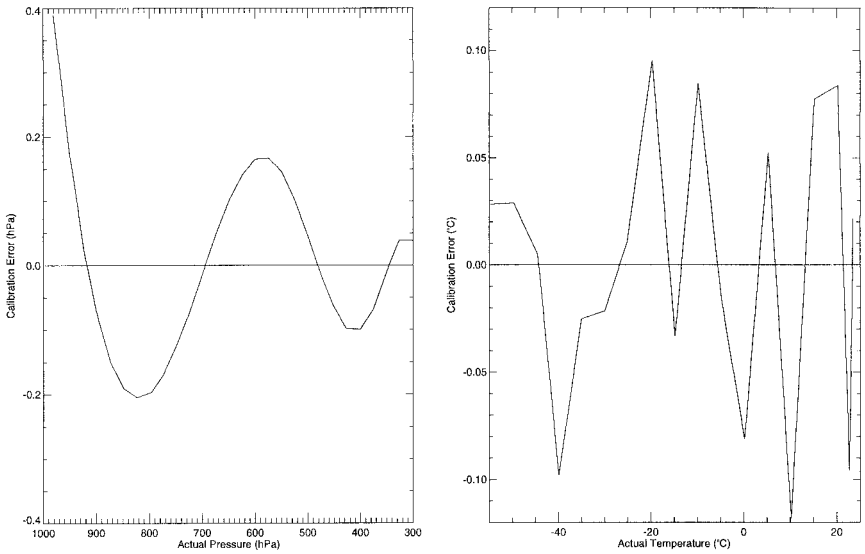

FIG. 7. Plots of the (a) pressure calibration error and the (b) temperature calibration error from actual measurements. Calibration errors are generally less than 0.20 hPa and 0.10°C for pressure and temperature.

3. Initial results

A three-balloon experiment was conducted on 16 August 1997 at the Clemson University Atmospheric Research Laboratory located near Clemson, South Carolina. Each of the three balloons was filled with sufficient helium to provide 1400 g of lift. The balloons were launched simultaneously at 1714 UTC from positions that were approximately 50 m apart. The data collected during the ascents are shown in Figs. 8a and 8b. The plot in Fig. 8a shows height versus temperature for the balloons. Altitudes were determined from the standard hydrostatic equation, assuming dry air. Also plotted in Fig. 8a are data from standard rawinsonde launches from three nearby NWS facilities. The data are plotted for both the 16 August 1200 UTC and the 17 August 0000 UTC NWS launches. The weather conditions in the surrounding region were dominated by a broad area of high pressure, with hot and humid summer conditions prevailing. At the time of the multiple-radiosonde launch, scattered cumulus clouds had developed with nearly calm surface winds. Differences between the NWS and multiple-radiosonde temperature data are attributed to the spatial and temporal differences between the sites. The majority of these differences are evident in the boundary layer, and since the multiple-radiosonde launch occurred during the peak afternoon heating of the surface, the temporal effects of solar heating are most pronounced. This can be seen clearly in Fig. 8b, in which the difference between the temperatures obtained from the NWS Peachtree City, Georgia, (FFC) radiosonde at 1200 UTC and the three simultaneously launched radiosondes at 1714 UTC are shown. Near the surface, the temperature difference between the NWS and multiple radiosondes exceeds 5.0°C. Temporal variations are not as pronounced higher in the atmosphere, and correspondingly, in this region the NWS and multiple-radiosonde differences are generally less than ± 2.0°C. The multiple-radiosonde temperature data show good correlation with each other, with slight variations due to the horizontal gradients in the temperature field. Comparisons of the pressure as a function height show extremely consistent results. The overall pressure and temperature profiles parallel closely the profiles obtained from the NWS launches.

To obtain the three-dimensional position of the radiosondes as they rose, a vertically pointing camera with a wide-angle lens was used to photograph the balloons at 3-s intervals. The photographic images were obtained with Nikon F3 HP cameras, using 250 exposure backs and either 24- or 16-mm lenses. The camera tripods were leveled prior to the balloon launches so that the centers of the images correspond to the zenith direction. The lenses have been calibrated using star fields during nighttime exposures to map the zenith angle as a function of radial distance on the photographs. The balloon locations can then be determined by combining the altitude information derived from the pressure and temperature measurements and the balloon positions in the images corrected for lens distortion. Figure 9 presents three images, taken during the launch, that show the three balloons at 21-s intervals. Note that the rate of change in the area of the triangle defined by the balloon positions is related to the horizontal divergence and thus to the vertical air motion. In the future, after proper

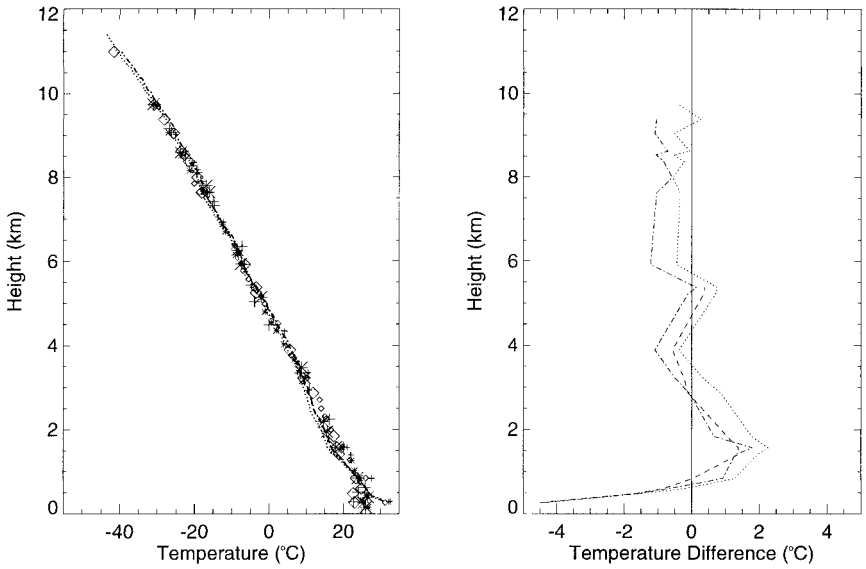

FIG. 8. Plot of (a) altitude versus temperature and (b) temperature difference of the three radiosondes from NWS temperature data from the 144- (dashed), 145- (dotted), and 147-MHz (dash–dotted) radiosondes and from nearby NWS rawinsodes at Peachtree City (◊) (FFC); Greensboro, North Carolina, (+) (GSO); and Morehead City, North Carolina (*) (MHX) on 16 August 1200 UTC (large symbols) and 17 August 0000 UTC (small symbols). In (b) the temperature difference is given between the NWS FFC launch at 1200 UTC and the three simultaneously launched radiosondes. A small difference is seen between the temperature values for the NWS and multiple balloons. This is attributed to the temporal and spatial differences between the launch sites. Furthermore, temporal solar heating effects are most evident in the boundary layer, since the Clemson University launch was at 1714 UTC. The three radiosondes launched from the Clemson University site show good agreement.

calibration of the optical system, work will include the actual calculation of the divergence.

4. Discussion of possible applications

If the three-dimensional position of the radiosondes is acquired, there are many applications for the new radiosonde system. One application is estimation of the horizontal pressure and temperature gradients. With the spatial separation of the three simultaneously launched radiosondes, detailed horizontal gradient measurements are acquired easily. These measurements allow isobars, isotherms, and isentropes to be determined within the spatial separation of the radiosondes. Various separations can be used to obtain different scale gradient measurements. Furthermore, the system easily can be expanded to include more transmitters, which would provide the redundancy needed for measurements that are more accurate. The transmitters have also been designed for the simple addition of other types of sensors.

Another of the atmospheric parameters that can be derived is that of the horizontal velocity divergence of the wind field. The horizontal velocity divergence of a flow moving with vector velocity **u** is determined from the following equation (Djurić 1994):

$$\nabla \cdot \mathbf{u} = \frac{1}{A} \int_L v_n \, dl, \tag{2}$$

where L is the contour surrounding the area A circumscribed by the balloons. The component of the flow normal to the contour is denoted by v_n. Horizontal velocity divergence can be approximated by how a predefined triangular area between the radiosondes changes with time. For a small change in time Δt, the divergence is given by

$$\nabla \cdot \mathbf{u} \cong \frac{1}{A} \frac{\Delta A}{\Delta t}, \tag{3}$$

where ΔA represents the change in the predefined triangular area A of the radiosondes after a time increment Δt.

The horizontal wind field can be obtained by monitoring the horizontal positions of the radiosondes over time. Using the zonal and meridional components of the wind field, horizontal inhomogeneities in the horizontal wind could be determined also. One of these is the vertical component of relative vorticity ζ given by

$$\zeta = \frac{1}{A} \int_L v_t \, dl, \tag{4}$$

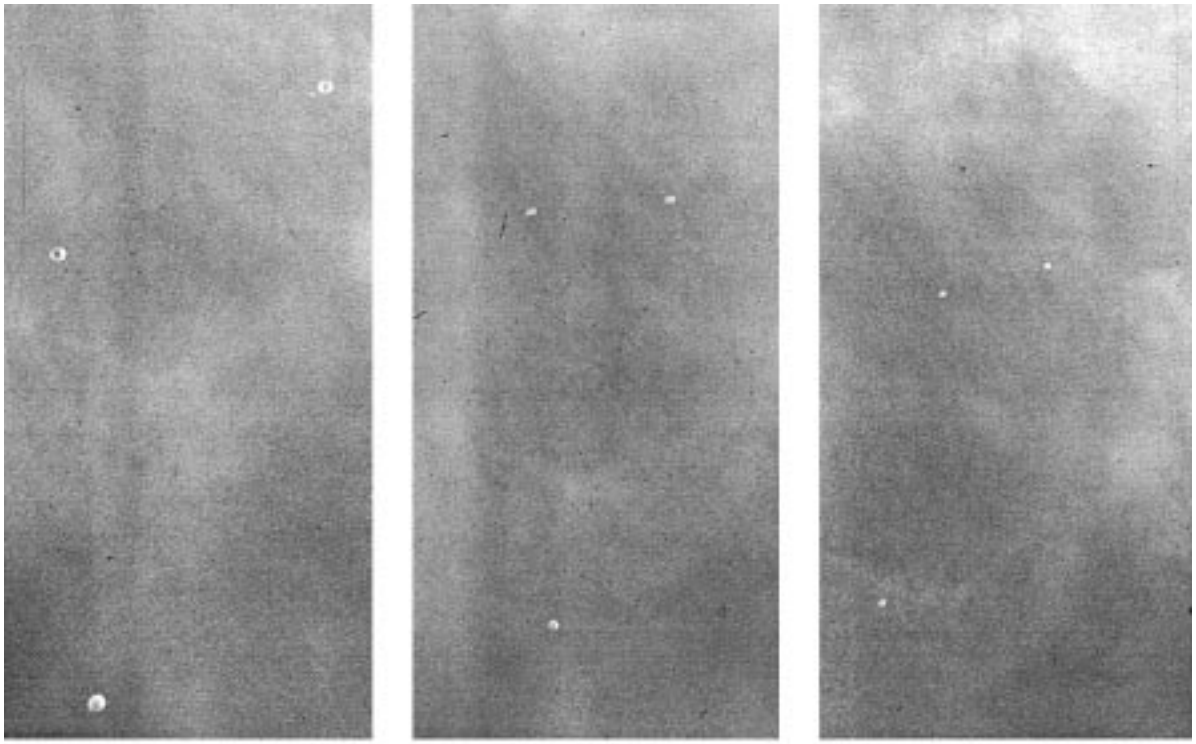

FIG. 9. A sequence of three images showing the three balloons at 20, 41, and 62 s after launch. The images are an enlarged portion of the original full image. Notice that the change in the area defined by the balloon locations is related directly to the wind field horizontal divergence and thus to the vertical velocity.

where v_t is the tangential wind component along the contour L surrounding area A. Other inhomogeneities that could be derived include both stretching and shearing deformations.

From the horizontal velocity divergence, and assuming no local density gradients, the vertical velocity of the wind can be obtained from the mass continuity equation

$$\frac{\partial w}{\partial z} = -\nabla \cdot \mathbf{u}, \tag{5}$$

where w is the vertical velocity and z is the height. Vertical velocity estimates obtained from an atmospheric radar—in particular, a boundary layer radar—could be compared to those calculated from the radiosonde system.

5. Conclusions

Radiosondes were chosen as the means to study the atmosphere because of the inherent advantages of in situ measurements. With the new radiosonde system that has been developed, small-scale horizontal gradients can be obtained in the temperature and wind fields. The simple design of the system allows this information to be acquired in a cost-effective manner. Other remote sensing technologies, such as Doppler radars, can be used to obtain estimates of horizontal flow gradients. However, the vertical component of relative vorticity cannot be obtained from single-Doppler radar systems. The initial goal of the new system was the in situ verification of Doppler radar vertical velocity measurements using the derived divergence estimates from the balloon network. However, many more applications have been envisioned since the initial design of the system. Preliminary data from the system were presented and show good correlation with NWS data. Future work will involve the calculation of the various inhomogeneities using the combination of the optical tracking system and radiosonde network.

Acknowledgments. BRC and RDP were partially supported by the Division of Atmospheric Sciences of the National Science Foundation through Grant ATM 94-02021, as well as by the Center for Electro-Optics at the University of Nebraska—Lincoln. MFL was supported by AFOSR Grant F49620-94-1-0440. The authors would like to thank S. Holweger, P. Hoffart, S. Schaffert, and J. Boyle for their assistance in the hardware construction. The authors would also like to thank P. Larsen, C. Ulbrich, and D. Hysell for their help during the launches in South Carolina.

REFERENCES

Corner, B., 1997: Measurements of wind field inhomogeneities in the planetary boundary layer using a radiosonde array. M.S. thesis, Dept. of Electrical Engineering, University of Nebraska at Lincoln, 77 pp. [Available from University of Nebraska at Lincoln Engineering Library, 204 W. Nebraska Hall, Lincoln, NE 68588-0516.]

Dalaudier, F., C. Sidi, M. Crochet, and J. Vernin, 1994: Direct evidence of ''sheets'' in the atmospheric temperature field. *J. Atmos. Sci.,* **51,** 237–248.

Djurić, D., 1994: *Weather Analysis.* Prentice-Hall, 304 pp.

Jasperson, W., 1982: Mesoscale time and space wind variability. *J. Appl. Meteor.*, **21,** 831–839.

United States Federal Aviation Administration, 1994: Federal aviation regulations. Part 101. Moored balloons, kites, unmanned rockets, and unmanned free balloons. United States Department of Transportation, Federal Aviation Administration, Washington, D.C., 5 pp. [Available from Federal Aviation Administration, 800 Independence Ave., S.W., Washington, DC 20591.]

——, 1995: *The FCC Rule Book: Complete Guide to the FCC Regulations Governing Amateur Radio.* 10th ed. The American Radio Relay League, 320 pp.